Fabrication of optical fiber sensor based on double-layer SU-8 diaphragm and the partial discharge detection*

SHANG Ya-na (商娅娜), **NI Qing-yan** (倪晴燕), **DING Ding** (丁丁), **CHEN Na** (陈娜)**, **and WANG Ting-yun** (王廷云)

Key Laboratory of Specialty Fiber Optics and Optical Access Networks, Shanghai University, Shanghai 200072, China

(Received 5 November 2014)

In this paper, a partial discharge detection system is proposed using an optical fiber Fabry-Perot (FP) interferometric sensor, which is fabricated by photolithography. SU-8 photoresist is employed due to its low Young's modulus and potentially high sensitivity for ultrasound detection. The FP cavity is formed by coating the fiber end face with two layers of SU-8 so that the cavity can be controlled by the thickness of the middle layer of SU-8. Static pressure measurement experiments are done to estimate the sensing performance. The results show that the SU-8 based sensor has a sensitivity of 154.8 nm/kPa, which is much higher than that of silica based sensor under the same condition. Moreover, the sensor is demonstrated successfully to detect ultrasound from electrode discharge.

Document code: A **Article ID:** 1673-1905(2015)01-0061-4

DOI 10.1007/s11801-015-4209-9

Optical fiber Fabry-Perot (FP) micro cavity sensors are widely used in static pressure measurement and ultrasound detection due to their advantages over traditional piezoelectric sensing technologies, such as small size, immunity to electro-magnetic interference (EMI) and high sensitivity. Among various configurations, diaphragm based extrinsic FP interferometric (EFPI) sensors are preferred in the applications with high sensitivity requirements, in which the diaphragm is a determinant of the sensitivity. Different materials have been proposed for EFPI sensing diaphragm, including silica[1-6], silicon[7-11], graphene diaphragm[12,13], polymer diaphragm[14-16] and sapphire wafer[17]. In this paper, we fabricate SU-8 diaphragm based EFPI sensor by photolithography, demonstrate its ultrasound detection ability, and compare its sensitivity with that of silica diaphragm based sensor by static pressure measurement and electrode discharge detection.

The schematic diagram of the FP pressure sensor is shown in Fig.1. The FP sensing element is mainly formed by a single mode fiber and a double-layer SU-8 diaphragm. The single mode fiber bonded with a ceramic ferrule is placed into a glass tube. The SU-8 diaphragm includes two layers, the inner is used to control the cavity length, and the outer is used to sense the pressure. The outer end face of the fiber and the inner surface of the SU-8 diaphragm are deposited with gold films with a reflectance of about 50%. Thus, air cavity is formed by these two gold film mirrors. The cavity length can be well controlled with photolithography method by tuning the thickness of the inner SU-8 layer.

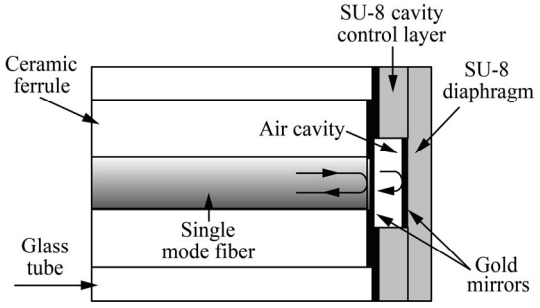

Fig.1 Structure of SU-8 diaphragm based optical fiber EFPI sensor

According to the interferometry theory, when a beam is injected in the FP sensing element, the reflected light from the sensor is a result of multi-interference in the FP cavity, and it can be simplified to the two-beam interference. The reflection intensity I_r can be described by[18]

$$I_r(\lambda)=\frac{R_1+R_2-2\sqrt{R_1R_2}\cos\varphi}{1+R_1R_2-2\sqrt{R_1R_2}\cos\varphi}I_i(\lambda), \quad (1)$$

where I_i is the incident light intensity, R_1 is the reflectance of the gold film on the fiber end face, R_2 is the reflectance of the gold film on the SU-8 surface, λ is the

* This work has been supported by the National Basic Research Program of China (No.2012CB723405), and the Science and Technology Commission of Shanghai Municipality (Nos.13510500300, 14DZ1201403 and 14511105602).

** E-mail: na.chen@shu.edu.cn

wavelength of light, and φ is the phase which can be expressed as

$$\varphi = \frac{4\pi nl}{\lambda}, \tag{2}$$

where n=1 is the refractive index of the air in the cavity, and l is the cavity length. When the ultrasound is applied on the SU-8 diaphragm, the diaphragm deflects and the cavity length l changes. As a result, the light intensity I_r is modulated by the ultrasonic signal. If the light intensity I_r is tracked, the ultrasonic sensing can be realized. Fig.2 shows our experimental setup for ultrasound sensing, in which a circuit composed of the photoelectric conversion and signal amplifier modules is used to track the light intensity I_r, and the signal demodulation is achieved. And finally, we can observe the ultrasonic electrical signal with an oscilloscope.

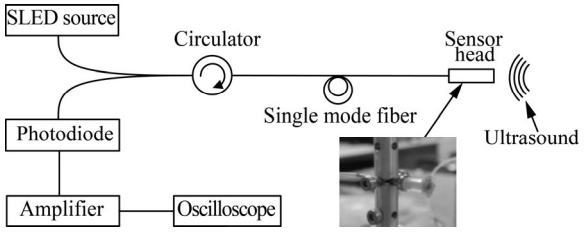

Fig.2 Experimental configuration of the SU-8 based EFPI sensor for ultrasound detection

For a diaphragm-based EFPI sensor, the sensitivity of the diaphragm per unit pressure is given by[19]

$$\eta = \frac{\mathrm{d}l}{\mathrm{d}p} = \frac{3(1-v^2)r^4}{16Et^3}, \tag{3}$$

where p is the pressure, v is Poisson's ratio (v=0.22 for SU-8 at 25 °C), E is Young's modulus of the SU-8 material (E=2.0 GPa at 25 °C), r is the effective radius of the diaphragm, and t is the thickness of the diaphragm. With the known values of the SU-8 material properties, the sensitivity of the SU-8 diaphragm can be written as

$$\eta = \frac{\mathrm{d}l}{\mathrm{d}p} \approx 8.9\times10^7 \frac{r^4}{t^3} \ (\mathrm{nm/kPa}), \tag{4}$$

where l is given in nanometers, p in kilopascals, r in millimeters and t in micrometers. In our design, the effective radius r is 0.7 mm, and a theoretical sensitivity curve is plotted in Fig.3. From Eq.(4), the sensitivity of the diaphragm with an effective radius of 0.7 mm and a thickness of 51 μm is 161.1 nm/kPa. The substituted parameters are the values used in our experiment. For comparing with the properties of silica based EFPI sensor, the sensitivity curve of the silica diaphragm is also plotted in Fig.3. Previous papers[6] have reported the sensitivity of silica diaphragm, and the sensitivity is given by

$$\eta = \frac{\mathrm{d}l}{\mathrm{d}p} \approx 2.5\times10^6 \frac{r^4}{t^3} (\mathrm{nm/kPa}). \tag{5}$$

As shown in Fig.3, the SU-8 diaphragm has a higher sensitivity than silica diaphragm, which is one of the reasons why we choose SU-8 as the pressure-sensing element. And in our experiment, we also fabricate a sensor head using a silica diaphragm with the effective radius of 1.25 mm and the thickness of 110 μm, and its theoretical sensitivity is 4.6 nm/kPa.

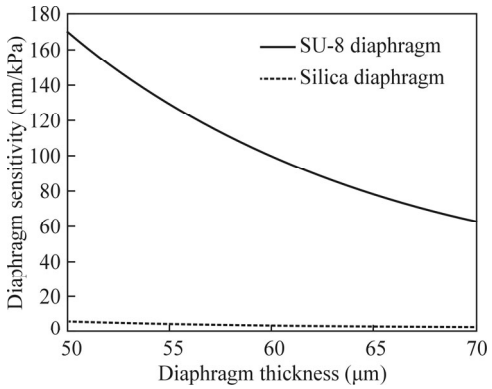

Fig.3 Diaphragm sensitivity versus diaphragm thickness for r=0.7 mm

For the design of cavity length, we need to further consider the experimental condition and the properties of the FP cavity. The light source is a super-luminescent light emitting diode (SLED) centered at 1 550 nm with a broad bandwidth from 1 400 nm to 1 700 nm and a maximum power of 20 mW. Fig.4(a) shows the optical spectrum of the SLED light source used in our sensing system. From Eqs.(1) and (2), with light source's spectrum shown in Fig.4(a) and R_1=R_2=50%, the interference fringe can be simulated as shown in Fig.4(b). From Fig.4(b), to avoid the phase sensitivity reduction, the cavity length of the sensor in one operating period should be restrained between two vertical dash lines, and it means that the sensor can work in a linear range. The point in Fig.4(b) means that when the initial cavity length is set to be the value corresponding to the point, the highest phase sensitivity and AC signal intensity of the sensor can be obtained.

During our fabrication process, we try to control the cavity length to be in the linear operating range as far as possible. For an air cavity, from Eq.(2), the phrase of the kth trough in the interference fringe can be written as

$$2k\pi = \frac{4\pi l}{\lambda_k}, \tag{6}$$

where λ_k is the wavelength of the kth trough. When the pressure applied on the diaphragm changes the cavity length, the trough in the interference fringe produces a corresponding shift. The relation between the change in cavity length Δl and the shift in trough $\Delta\lambda_k$ can be expressed as

$$\Delta\lambda_k = \frac{2}{k}\Delta l. \tag{7}$$

It can be seen from Eq.(7) that for a determined Δl, smaller k can gain a larger trough shift, which also leads to larger phase shift and phase sensitivity. From Eq.(6), for a known wavelength of trough, k is in direct proportion to the cavity length l. If we hope to make k smaller to get a higher phase sensitivity, a sensor with a small cavity length can be made.

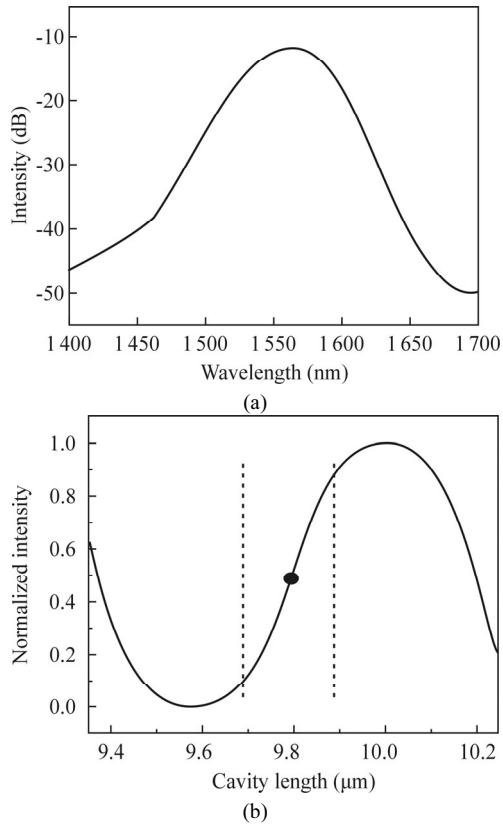

Fig.4 (a) Optical spectrum of the SLED source; (b) Simulated result of the interference fringe with the SLED source

Based on our design, two sensors with similar structure are fabricated and tested for comparison. One is with a 51 μm-thick SU-8 diaphragm and a cavity length of 13 μm, while the other one is with a 110 μm-thick silica diaphragm and a cavity length of 19 μm. The experimental system for the static pressure measurement is similar to that shown in Fig.2. To obtain the sensitivity of the EFPI sensor, both sensors are immersed into the water tank at different depths, and an optical spectrum analyzer (OSA) is used to measure the optical spectrum reflected from the sensor. The sweep range of the OSA is set to be from 1 400 nm to 1 650 nm, while the sampling interval is 0.05 nm. There are 5 001 sampling points, and the sensitivity is HIGH2. Besides, a computer with Matlab program is connected to the OSA to process the optical spectrum data.

In the static pressure experiments, the sensors are immersed in a water tank at different depths from 4 cm to 12 cm, and the corresponding interference fringe spectra are recorded and processed. Fig.5 shows the pressure responses of the two sensors.

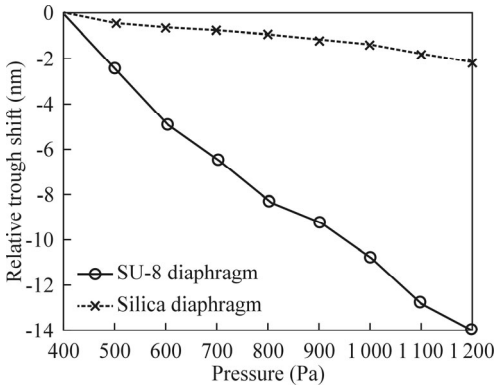

Fig.5 Static pressure responses of SU-8 diaphragm based sensor and silica diaphragm based sensor

From Fig.5, we can see that the trough in the SU-8 interference spectrum shifts by about 2 nm, while that for the silica shifts by about 0.45 nm with pressure change of 100 Pa in static pressure. From the experiment, the high sensitivity of 154.8 nm/kPa is achieved for the SU-8 diaphragm based EFPI sensor. This sensitivity is much higher than that of the silica diaphragm based EFPI sensor, which is consistent with the theoretical results.

The experimental system for the ultrasound detection is illustrated schematically in Fig.2. The light from the SLED is first launched into the single mode fiber, and reaches the sensor head through an optical circulator. Then the interference light is modulated by the ultrasound, and travels back into a photodiode. After the photodiode, the electrical signal is amplified and displayed on an oscilloscope. In the ultrasound detection experiment, the sensors are used to detect the ultrasound in the air, which is generated by a simulated high voltage discharge. Fig.6(a) shows the sensor arrangement in the discharge detection experiments. An SU-8 diaphragm based sensor and a silica diaphragm based sensor are separately located around the electrode discharge source. The right sensor in Fig.6(a) is the SU-8 sensor, which is 16.5 cm away from the discharge source, while the other sensor is the silica one and the distance from the source is 5 cm. The demodulation circuit with a pass band of 150–220 kHz includes two signal detection channels which can simultaneously receive the ultrasound signals detected by two sensors. The waveforms of the detected signals are given in Fig.6(b).

As shown in Fig.6(b), the signal detected by the silica diaphragm based sensor, which is closer to the discharge source, first reaches the circuit, and the cost time is nearly 140 μs, while the signal detected by the SU-8 one arrives later, and the cost time is nearly 480 μs. The velocity of the ultrasound in air is known to be about 340 m/s, so the distances between the sensors and the discharge source can be separately calculated to be 4.76 cm and 16.32 cm, which are close to the previously set distances of 5 cm and 16.5 cm.

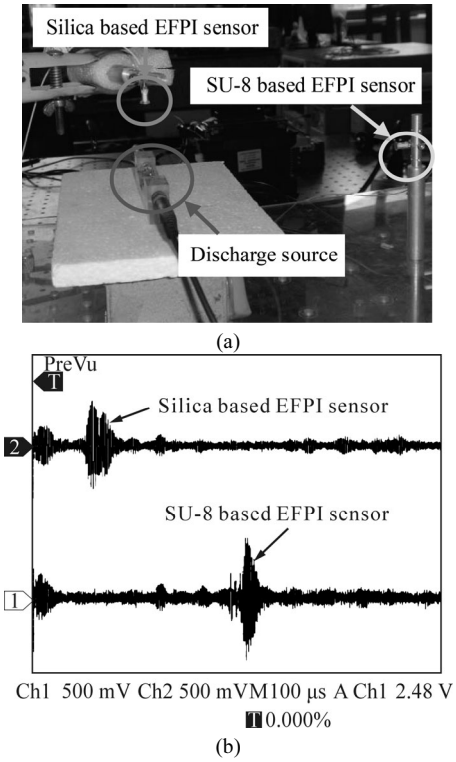

Fig.6 (a) Photograph of the experimental setup; (b) Ultrasonic signals detected by SU-8 diaphragm and silica diaphragm based sensors

To sum up, an optical fiber FP sensor based on double-layer SU-8 diaphragm is developed for partial discharge detection in this paper. The SU-8 material is chosen to make the diaphragm since the low Young's modulus of SU-8 can lead to a higher sensitivity for pressure sensing. Moreover, with the use of traditional photolithography, the sensor can be easily fabricated, and the cavity length can be well controlled. With two reflective surfaces coated with gold film, the fringe contrast of the FP cavity is improved. Experimental results demonstrate that the sensor has a high sensitivity and shows a good linearity and high resolution for static pressure measurement. Moreover, the sensor has been proved to successfully detect ultrasound from both piezoelectric ceramics (PZT) and electrode discharge.

References

[1] ZHU Jia-li, WANG Ming, YANG Chun-di and WANG Ting-ting, Optoelectronics Letters **9**, 85 (2013).

[2] LI Li-tong, ZHANG Dong-sheng, WEN Xiao-yan and LI Xiong, Journal of Optoelectronics·Lasers **25**, 2130 (2014). (in Chinese)

[3] Denis Donlagic and Edvard Cibula, Optics Letters **30**, 2071 (2005).

[4] Xingwei Wang, Juncheng Xu, Yizheng Zhu, Kristie L. Cooper and Anbo Wang, Optics Letters **31**, 885 (2006).

[5] Ming Han, Xingwei Wang, Juncheng Xu, Kristie L. Cooper and Anbo Wang, Optical Engineering **44**, 060506-1 (2005).

[6] Bing Yu, Dae Woong Kim, Jiangdong Deng, Hai Xiao and Anbo Wang, Applied Optics **42**, 3241 (2003).

[7] Junfeng Jiang, Tiegen Liu, Kun Liu, Lijuan Jiang, Xiao Liang, Yu Liu, Meng Wang, Cong Xu, Yimo Zhang and Xuejin Li, Optical Fiber Fabry-Perot Pressure Sensor Machined by Nd:YAG Laser, 9th International Conference on Optical Communications and Networks, 112 (2010).

[8] Cheng Pang, Hyungdae Bae, Ashwani Gupta, Kenneth Bryden and Miao Yu, Optics Express **21**, 21829 (2013).

[9] LIU Yu, WANG Meng, WANG Bo, JIANG Li-juan and WANG Shao-hua, Transducer and Microsystem Technologies **32**, 112 (2013). (in Chinese)

[10] Xiaodong Wang, Baoqing Li, Zhixiong Xiao, Sang Hwui Lee, Harry Roman, Onofrio L. Russo, Ken K. Chin and Kenneth R. Farmer, Journal of Micromechanics and Microengineering **15**, 521 (2005).

[11] WANG Wei, WANG Zan, WU Yankun, DU Jiazhen and LI Fuping, High Voltage Engineering **40**, 814 (2014). (in Chinese)

[12] Jun Ma, Wei Jin, Hoi Lut Ho and Ji Yan Dai, Optics Letters **37**, 2493 (2012).

[13] Jun Ma, Haifeng Xuan, Hoi Lut Ho and Ji Yan Dai, IEEE Photon. Technol. Lett. **25**, 932 (2013).

[14] H. Bae and M. Yu, Optics Express **20**, 14573 (2012).

[15] H. Bae, X. M. Zhang, H. Liu and M. Yu, Optics Letters **35**, 1701 (2010).

[16] Qiaoyun Wang, Jianwei Wang, Liang Li and Qingxu Yu, Sensors and Actuators B: Chemical **153**, 214 (2011).

[17] Jihaeng Yi, Evan Lally, Anbo Wang and Yong Xu, IEEE Photon. Technol. Lett. **23**, 9 (2011).

[18] Heavens O. S., Optical Properties of Thin Solid Films, Courier Dover Publications, 1991.

[19] Giovanni D., Flat and Corrugated Diaphragm Design Handbook, CRC Press, 1982.